ELSEVIER

Polymer 41 (2000) 1541–1550

polymer

Crystallization in isotactic polypropylene melts during contraction flow: time-resolved synchrotron WAXD studies

U. Göschel*, F.H.M. Swartjes, G.W.M. Peters, H.E.H. Meijer

Eindhoven Polymer Laboratories (EPL), Eindhoven University of Technology, PO Box 513, 5600 MB Eindhoven, The Netherlands

Received 7 December 1998; received in revised form 25 February 1999; accepted 26 March 1999

Abstract

Time-resolved 2D WAXD studies have been performed on α-nucleated isotactic polypropylene (iPP) in order to study the development of crystal growth and crystallite orientation during and subsequent to contraction melt flow at elevated temperatures in the range from 159 to 172°C. Prior to flow, an annealing procedure is carried out at 230°C for 90 min to erase memory effects in terms of crystal aggregates and molecular conformations. The onset of crystallization is visible at temperatures as high as 170°C, which is far above the crystallization range under quiescent conditions. Depending on the applied flow rates mainly two different crystalline orientations are observed. A low flow rate $\dot{\gamma} = 9.1\ s^{-1}$ at 159 and 161°C causes intensive meridional (110) and equatorial (040) reflections during flow (95–140 s) which can be described by lamellar branching via homoepitaxy. Whereas with increasing flow rate up to $\dot{\gamma} = 127.1\ s^{-1}$ the equatorial *hk*0 reflections become dominant, indicating a preferential orientation of crystallites with their *c*-axis in flow direction.

Keywords: Isotactic polypropylene; Flow-induced crystallization; Synchrotron X-ray diffraction

1. Introduction

Thorough knowledge about the behavior of polymer melts during flow is essential to control both industrial flow processing conditions and resulting product properties. New insights in the complex influence of the thermo-mechanical history, experienced during processing, on final properties can be expected from time-resolved X-ray studies in combination with advanced numerical models to describe the morphological changes during and after flow.

Different approaches were made to study the solidification process. Among them are rheological and microstructural investigations applying special devices for shear (e.g. Janeschitz-Kriegl and co-workers [1–4]) and elongational flow (e.g. Mackley and Keller [5,6] and Mackey et al. [7]).

Recently, the influence of total shear ($\gamma = \dot{\gamma}t$) on isothermal crystallization of iPP of different molecular weight and distribution was monitored by Vleeshouwers and Meijer [8]. They applied a shear rate of $5\ s^{-1}$ in the temperature range from 200 to 260°C, thereafter, cooled down to the crystallization temperature (138 and 140°C) and measured the development of the storage modulus G' and loss angle tan δ in time in a range up to 4500 s by means of a standard rheometer (Rheometrics RDS2) with a cone and plate configuration. Shearing in the melt enhances subsequent crystallization at lower temperatures. Shear rate and time revealed independent influences on crystallization. Short times at high rates were found to be most effective. Furthermore, it was documented that the crystallization behavior is very sensitive to molecular weight and distribution.

In the case of shear flow, Janeschitz-Kriegl and co-workers [1–4] have suggested a model to describe nucleation and growth kinetics. This theory provides the possibility to determine kinetic parameters from independent experiments [9]. Contrary to that, extensional flow-induced crystallization in confined geometries is less explored [5–7]. The lack of knowledge is mainly due to a large sensitivity of the above crystallization type to small flow and temperature variations which rises problems to control the structural development [5–7,10].

Keller and co-workers [11] discussed the phase transformations of linear polyethylene in the course of contraction flow using time-resolved synchrotron X-ray experiments at the DESY in Hamburg. The same flow cell, together with a different set-up for heat and pressure control, is applied on isotactic polypropylene (iPP) in our present paper.

Isotactic polypropylene is known to crystallize in different unit cell modifications. The most common structure is

* Corresponding author. Tel.: +31-40247-3079; fax: +31-40243-6999.
E-mail address: u.goeschel@tue.nl (U. Göschel)

0032-3861/00/$ - see front matter
PII: S0032-3861(99)00303-1

the monoclinic α-form which is also the most stable modification under atmospheric pressure. According to Natta et al. [12] and Turner-Jones et al. [13], the crystal unit cell can be described by $a = 0.665$ nm, $b = 2.078$ nm, $c = 0.6495$ nm, $\beta = 99.6°$ and $\alpha = \gamma = 90°$. The α-modification shows the following X-ray reflections ($2\theta_{Cu}$): 14° (110), 17° (040), 18.5° (130), 21° (111) and 22° ($\bar{1}31$), (041) [12]. The hexagonal β-unit cell structure, represented by the $2\theta_{Cu}$ reflections 16° (300) and 21° (301) [13], can be obtained by a high orientation or deformation in the melt [14], high crystallization temperatures [15], large temperature gradients [16] or presence of special nucleation agent [17]. The triclinic γ-form is mainly formed under elevated pressure [18] or by the crystallization of low molecular weight iPP [19]. Turner-Jones et al. [13] reported about a characteristic reflection at 20.1° ($1\bar{2}0$), which is absent in the α-phase. However, small portions of the γ-form are often observed in association with the α-phase [20].

Clark and Spruiell [21] reported about a unique behavior of iPP when it crystallizes from a melt under extensional flow conditions. They studied the structure development during melt spinning of iPP by means of on-line wide angle X-ray diffraction (WAXD) measurements. Using a 6 kW rotating anode generator the diffraction patterns were obtained as a function of distance from the spinneret for a running monofilament. SAXS measurements were performed on the final spun fibers by means of e.g. a pinhole goniometer technique. From the WAXD patterns showing a simultaneously arcing of the (110) reflection along the meridian as well as the equator together with a sharp two-point SAXS pattern it was concluded the existence of two different and independent orientations of the unit cell, one component with the *c*-(chain) axis parallel and the second one perpendicular to the flow direction and called it a *bimodal orientation*.

The chain conformation of iPP in the crystalline state is described by a right- and left-handed three-fold helices with a periodicity of 6.5 Å. Due to different modes of packing of the chiral chains along the *c*-axis, the highly unusual capability of homoepitaxy is given in terms of the coexistence of different chain axis directions within the same lattice [22–26]. It is well-documented that homoepitaxy on the lateral *ac*-faces of α-phase iPP may cause lamellar branching, when the sequence of alternately left- and right-handed molecular chain helices in successive (040) planes is disturbed [26]. A tilt angle of 80° between daughter and original parent lamella is determined [25,26]. Recently, Hikosaka and coworkers [27] discussed the cross-hatching in iPP with respect to the role of configurational defects within a molecular chain and the mobility of molecules in the crystallization process. Applying polarizing optical as well as transmission electron microscopy they ascertained a decrease in cross-hatching within a spherulite with an increase in isotacticity and crystallization temperature.

The crystallization process is widely recognized as kinetically controlled. Below the equilibrium melting temperature (T_m^0), the polymer system will spontaneously minimize its free Gibbs energy *G* by crystallization, which involves nucleation and crystal growth. *G* is defined as $G = H - TS$, where *H*, *S* and *T* are the specific enthalpy, entropy and absolute temperature, respectively. Consequently, the driving force of crystallization is determined by the excess of the thermodynamic free energy of the system which means for stretched polymer molecules a decrease in the entropy is caused by chain orientation. Experiments show clearly that the logarithm of the linear crystal growth rate is proportional to $1/(T_c\Delta T)$, where T_c is the crystallization temperature and $\Delta T = T_m^0 - T_c$ the undercooling. Furthermore, the thickness of the lamellar crystal is inversely related to the undercooling ΔT. The presence of a nucleating agent supports a heterogeneous nucleation, which always takes place at a lower undercooling than homogeneous nucleation. The two phenomena, nucleation and crystal growth without any volume constraints, can be described by temperature-dependent expressions (kinetic theories) which enable to predict the temperature dependence of growth rate and initial crystal thickness. Recently, the spinodal decomposition is reported to describe the early stage of crystallization in supercooled polymer melts [28,29]. It is proposed that a coupling between density and chain conformation induces a liquid–liquid binodal within the equilibrium liquid–crystalline solid coexistence region. However, a general growth theory which describes the development of crystalline morphologies under flow conditions, applicable to e.g. injection molding processes, is still in progress [1–4]. Despite several flow studies which have been performed in the last few years, the effect of flow-induced nucleation that enhances crystallization is still an open issue [8]. This is mainly due to the complexity of the problem such as a flow with portions of elongational and shear flow, the temperature control, the required combination of methods to analyze nucleation and crystal growth with temperature and time, the influence of tacticity, molecular conformation, molar mass and distribution.

The purpose of the present paper is to investigate the occurrence of crystallization at relatively high temperature as a consequence of flow-induced chain orientation in the melt. Defined flow conditions together with a high flux synchrotron WAXD set-up at the ESRF in Grenoble will be applied to describe effects of temperature and flow rate on the formation of oriented crystals and lay the groundwork for further flow studies.

2. Experimental

2.1. Materials

The flow experiments were carried out on α-nucleated isotactic polypropylene (iPP) Daplen K2 XMOD injection molding grade from Borealis AG, Linz, Austria. Gel

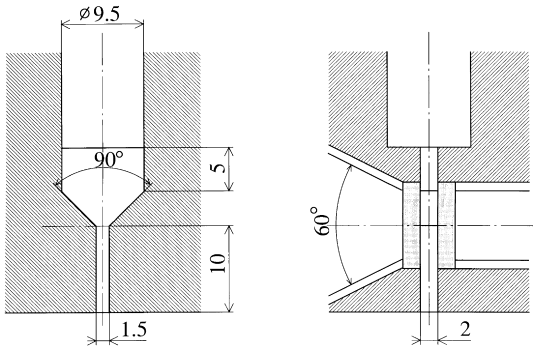

Fig. 1. Contraction flow cell [8].

permeation chromatography (GPC) measurements [30] in TCB at 135°C indicated a weight average molecular weight $M_w = 365$ kg/mol and a polydispersity $M_w/M_n = 5.45$. The melt flow index is 8.0 g/10 min and the isotacticity [mmmm] has been determined to be 97.2 mol% [30]. Prior to the flow experiment, rod-shaped preforms of about 9.5 mm in diameter were prepared [31].

2.2. Flow cell

Time-resolved wide angle X-ray diffraction (WAXD) experiments were performed during melt flow using a contraction flow cell which was applied in earlier studies on polyethylene by Kolnaar and Keller [11]. The cell consists of a cylindrical reservoir (diameter 9.5 mm, length 160 mm), and a contraction zone with a 90° entry angle to a slit-shaped die of 1.5×2.0 mm^2 and 10 mm in length (Fig. 1). At both sides of the slit a X-ray transparent beryllium window of 2 mm in thickness was used. The experimental parameters piston displacement and capillary temperature in the contraction zone were measured with an accuracy of ± 0.6 mm and ± 0.6°C, respectively. These parameters were recorded in time using a computer (with a measuring card "LabPC+" from National Instruments). The piston was moved by means of a hydraulic system using a hydraulic cylinder with a stroke of 100 mm. The piston velocity is calculated from the measured displacement. A Hasco heating unit (type Z126/2/10/N) was used for the electrical heating of the flow cell.

2.3. Flow experiments

Each of the flow experiment started with a fresh preform which was inserted in the flow cell at about 100°C. Thereafter, the temperature was raised towards $T_m = 230$°C and held for about $t_m = 90$ min to ensure an isotropical melt, free of any memory effects associated with clusters, crystal aggregates [32] and molecular conformation due to temperature and deformation history. Subsequently, the flow cell was cooled (rate 6°C/min) to the desired flow temperature by blowing air. The crystallization temperature (T_c), in the range from $159 \leq T_c \leq 172$°C was kept constant during the observation time (see Table 1). The piston velocity (v), which could be adjusted by means of a throttle valve (Bosch), was chosen in the range between 35 and 484 mm/min. A corresponding characteristic shear rate $\dot{\gamma}$ ranging from 9.1 to 127.1 s^{-1} has been determined according to $\dot{\gamma} = (vA_1)/(HA_2)$, where A_1 and A_2 are the area of the cylindrical reservoir and the outlet area of the contraction zone (measuring point), respectively, and H is the channel height of the slit-shaped die.

2.4. X-ray studies

WAXD measurements were carried out on the Material Science beamline BL2, ID-11 of the European Synchrotron Research Facilities (ESRF) in Grenoble, France. The X-ray beam was set to a wavelength of $\lambda = 0.0757$ nm and a size of 0.3×0.3 mm^2. The flow cell was placed vertically,

Table 1
Experimental flow conditions

Crystallization temperature (°C)	Shear rate $\dot{\gamma}$ in s^{-1} (flow time t_{fl} in s)		
	Low 9.1–16.0 ($165 \geq t_{fl} \geq 89$)	Medium 39.1–67.3 ($41 \geq t_{fl} \geq 19$)	High 110.3–127.1 ($14 \geq t_{fl} \geq 12$)
172.0	16.0[a]		122.9[b]
	15.4		
170.2	13.9		
167.7	11.6		
165.8	13.9		
163.4			110.3
			120.0[c]
161.1	11.8[d]	39.1	
		67.3	
159.2	9.1		127.1

[a] $t_m = t_c = 30$ min.
[b] $t_c = 90$ min.
[c] $t_c = 120$ min.
[d] $t_c = 150$ min.

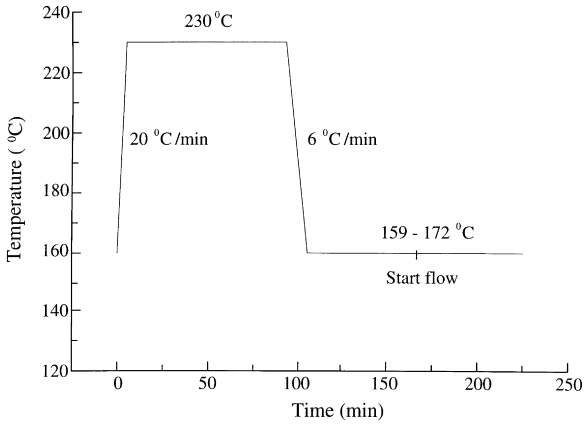

Fig. 2. Thermal conditions during the flow experiment.

perpendicular to the horizontal incident X-ray beam. Operating in transition mode with a sample thickness of 2 mm, the beam was centered in the entrance of the quadratic-shaped capillary. The 2D diffraction images were obtained by means of a Princeton CCD camera. A rebinning of the data enabled a data acquisition as short as 5 s. This is important with respect to the duration of flow ranging from 12 to 165 s depending on the applied flow rates. Usually, 3 scans were taken prior flow, followed by 40 scans with an interval (Δt) of about 5 s (covering the duration of flow) and finally, about 30 scans with $\Delta t = 120$ s. The ESRF program FIT2D (version 9.160) has been used for the data treatment. The detector intensities were spatially corrected by means of a grid scan as described in Hammersly [33]. The tilt of the detector and the beam center have been fitted to the Debye rings of one of our crystalline pattern.

3. Results

The flow experiment can be divided into three parts: preparation of preforms at $T_m = 240$°C and $t_m = 40$ min, annealing under melt conditions at $T_m = 230$° and $t_m = 90$ min to erase memory effects and finally, creation of flow at $T_c = 159$–172°C and studying isothermal crystallization by time-resolved X-ray investigations (Fig. 2).

3.1. Thermal conditions

Starting with the as-delivered iPP granulate, the first thermal loading was given by the preparation of rod-like preforms at 240°C and 40 min under standard conditions [29]. Vacuum was used to prevent oxidation.

Prior to flow, the fresh-inserted preform was annealed at $T_m = 230$°C for about $t_m = 90$ min to eliminate any memory effects [32]. It is known that for e.g. entanglement density increases and local order decreases with melting temperature and time. The annealing temperature of $T_m = 230$°C is about 65°C above the melting temperature but still below thermal degradation. Additional X-ray and calorimetric studies [34] have shown that these annealing conditions are sufficient to erase the polymer history.

The temperature during flow (T_{fl}) and the crystallization temperature (T_c) were chosen to be identical. The used temperatures (159–172°C) are high and close to the melting range of a quiescent melt. Consequently, the undercooling $T_m^0 - T_c$ with the equilibrium melting temperature T_m^0 of 187.6°C (Wunderlich and coworkers [35]) is rather low and will cause large times for nucleation and crystal growth under quiescent conditions. It is anticipated that crystallization can be enhanced significantly by flow-induced chain orientation with increasing flow rate.

3.2. Flow conditions

Subsequent to annealing under melt conditions to erase memory effects, capillary flow was created at different temperatures and flow rates. The temperature of flow was chosen in the range between 159 and 172°C with increments of about 2°C. The flow rate, characterized by the shear rate ($\dot{\gamma}$), has been classified as low ($9.1 \le \dot{\gamma} \le 16.0\ s^{-1}$), medium ($39.1 \le \dot{\gamma} \le 67.3\ s^{-1}$) and high ($110.3 \le \dot{\gamma} \le 127.1\ s^{-1}$). The flow rate determines the duration of the melt in the flow cell from 12 to 165 s (Table 1). This is the time range where crystallization during flow can be observed. The piston displacement was recorded and showed to be linear with time. Each flow experiment started with a new preform. The WAXD patterns which were taken prior to flow are always noncrystalline and characterize an isotropic melt. Different annealing times prior to flow have shown no effect on the crystallization behavior during and after flow.

3.2.1. Low flow rate

No crystallization is found during flow at low flow rates $\dot{\gamma} = 15.4$ and $16.0\ s^{-1}$ at 172°C. The applied temperature is well above the melting temperature of a quiescent melt. Calorimetrical (DSC) measurements in the second heating run at a rate of 10°C/min provide an endothermic melting peak of 170°C in the range from 113°C (onset) to 177°C (offset) [34]. Obviously, the undercooling $T_m^0 - T_c$ is too small, even for the oriented melt, and the available time for crystal growth is too short to detect any crystallization during flow at $T_c = 172$°C.

WAXD experiments show the onset of crystallization with the growth of a weak crystalline (110) reflection during flow at 170°C and a low flow rate $\dot{\gamma} = 13.9\ s^{-1}$. However, subsequent to flow the crystalline WAXD pattern turns into a noncrystalline one because the achieved chain conformation was not thermally stable enough. The decrease in pressure with the stoppage of flow may cause a decrease in the melting temperature [36] which finally enhances the tendency towards a melt. A similar behavior is found at 168°C and $\dot{\gamma} = 11.6\ s^{-1}$ as well as at 166°C and $\dot{\gamma} = 13.9\ s^{-1}$.

With a further decrease in temperature towards 159°C the

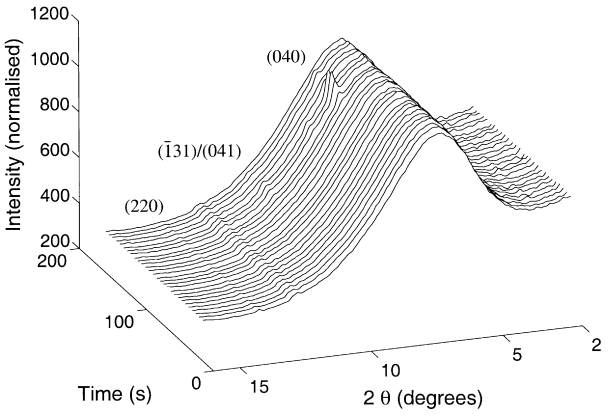

Fig. 3. Equatorial WAXD intensity of iPP vs. diffraction angle 2Θ and time during flow at 159°C and a low flow rate $\dot{\gamma} = 9.1\ s^{-1}$.

crystal growth accelerates during the duration of flow. This correlates with an increase in the undercooling $T_m^0 - T_c$ which determines the rate of nucleation and crystal growth. It is remarkable that the WAXD patterns during flow ($0 \leq t_{fl} \leq 165$ s) at 159 and 161°C change with time from noncrystalline to crystalline, reach a maximum intensity in the range from 95 to 140 s and turn back into a noncrystalline structure. Obviously, there is a competition between crystal growth and melting.

At 159 and 161°C, the WAXD patterns as a consequence of flow, under comparable flow rates, show only minor differences. The diffraction intensities tend to be somewhat larger in the case of the lower flow temperature. However, the crystallization kinetics and the resulting morphologies are almost identical. Therefore, the WAXD patterns obtained at 159°C and $\dot{\gamma} = 11.6\ s^{-1}$ will be used to explain the characteristics of the crystallization behavior at 159 and 161°C under low flow rates. Figs. 3 and 4 represent the crystal growth with time at 159°C along the equator and meridian (in flow direction), respectively. The formation of crystalline peaks takes place simultaneously along the equator and meridian. Dominant are the equatorial

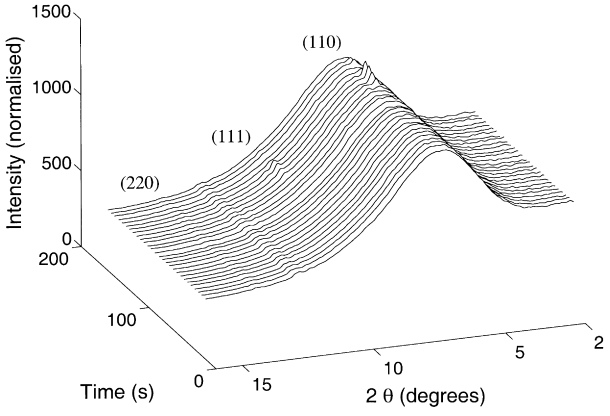

Fig. 4. Meridional WAXD intensity of iPP vs. diffraction angle 2Θ and time during flow at 159°C and a low flow rate $\dot{\gamma} = 9.1\ s^{-1}$.

$2\theta = 6.9°$ (040) (Fig. 3) and the meridional $2\theta = 8.3°$ (110) reflections (Fig. 4). The small peak at $2\theta = 12.45$ (at $\lambda = 0.0757$ nm) relates to an artifact due to the flow cell set-up. It occurs at a fixed angular position in the patterns prior to crystallization as well as in different materials. The arcing of the (040) and (110) reflections is significant and represented in Fig. 5. The 2D pattern corresponds to a scan taken during flow at $t = 134$ s, a time where the peak intensity is a maximum, seen in Figs. 3 and 4. The corresponding 1D plot (Fig. 6) shows the equatorial and meridional intensity distribution. Additional but weak reflections are: the meridional $2\Theta = 10.4°$ (111), 10.7° ($\bar{1}31$)/(041) and 13.9° (220) as well as the equatorial $2\Theta = 6.9°$ (110), 9.1° (130), 10.7° ($\bar{1}31$)/(041) and 13.9° (220) reflections. The peak positions are characteristic for a monoclinic α-modification.

The anisotropy in the crystallite orientation is significantly expressed by an arcing of the meridional (110) and equatorial (040) reflections (Figs. 3–6). As is known, the *hk*0-reflections represent lattice planes parallel to the *c*-(chain) axis which coincides with the main flow direction in our set-up. Consequently, the (040) intensity distribution along the equator indicates the expected crystallite orientation in flow direction. Contrary to that, the meridional (110) intensity is uncertain. However, an explanation can be given referring to Padden et al. [23] and Lotz et al. [24]. They described the occurrence of the meridional reflection by means of a homoepitaxy on the lateral *ac*-faces of the α-phase which causes lamellar branching of crystallites in the daughter lamella with their a^*-axis (originated by the *a*-axis of the daughter lamella) in flow direction [20]. The observed structural anisotropy based on the equatorial (040) and meridional (110) reflections is schematically drawn in Fig. 7. Probably, the *c*-axis orientation is a part of this structure.

3.2.2. Medium flow rate

Two flow rates at 161°C, which are classified as medium, with $\dot{\gamma} = 39.1\ s^{-1}$ and $\dot{\gamma} = 67.3\ s^{-1}$ (Table 1) provided a total flow duration of 41 and 19 s, respectively. The WAXD patterns for $\dot{\gamma} = 67.3\ s^{-1}$ show an onset of crystallization at about 17 s together with the formation of equatorial (110) and (040) reflections (Fig. 8(a)) and a meridional (110) reflection (Fig. 9(a)). Compared to $\dot{\gamma} = 67.3\ s^{-1}$, the flow rate of $\dot{\gamma} = 39.1\ s^{-1}$ yields a similar crystallization behavior, however the resulting degree of crystallinity is somewhat lower. The (110) reflection reveals an arcing along the equator as well as the meridian which is characteristic for the existence of a lamellar branching as previously described in the case of low flow rates.

Subsequent to flow, the crystallization continues in the measured time range up to 60 min. Immediately after stopping the flow (about 60 s), an intensity maximum at $2\theta = 13.9°$ is found for both of the medium flow rates, $\dot{\gamma} = 39.1\ s^{-1}$ and $\dot{\gamma} = 67.3\ s^{-1}$. The corresponding

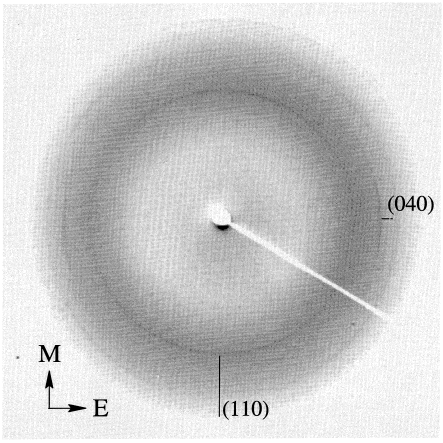

Fig. 5. 2D WAXD pattern of iPP during flow at 159°C, $t = 134$ s and a low flow rate $\dot{\gamma} = 9.1\ s^{-1}$. The flow direction is vertical.

d-spacing of 3.1 Å is most likely associated with the (220) reflection.

Starting from $t = 182$ s ($\dot{\gamma} = 67.3\ s^{-1}$) and 1382 s ($\dot{\gamma} = 39.1\ s^{-1}$) crystal growth takes place steadily with the formation of the known reflections of the monoclinic α-modification. However, the equatorial reflections (Fig. 8(b)) are more intense than the meridional ones (Fig. 9(b)).

The structural anisotropy which is obtained at 3035 s ($\dot{\gamma} = 67.3\ s^{-1}$) and 3083 s ($\dot{\gamma} = 39.1\ s^{-1}$) subsequent to flow is represented in Figs. 10 and 11. Those times correspond to the end of the observation time showing the highest diffraction intensities. A medium flow rate of $\dot{\gamma} = 67.3\ s^{-1}$ affects the formation of intense equatorial (110), (040) and (130) reflections, whereas the meridional reflections are only weak. The arcing of the three *hk*0 reflections indicates an alignment of the crystallites with their *c*-axis in flow direction. At the lower medium flow rate of $\dot{\gamma} = 39.1\ s^{-1}$, only a weak equatorial (110) reflection is observed.

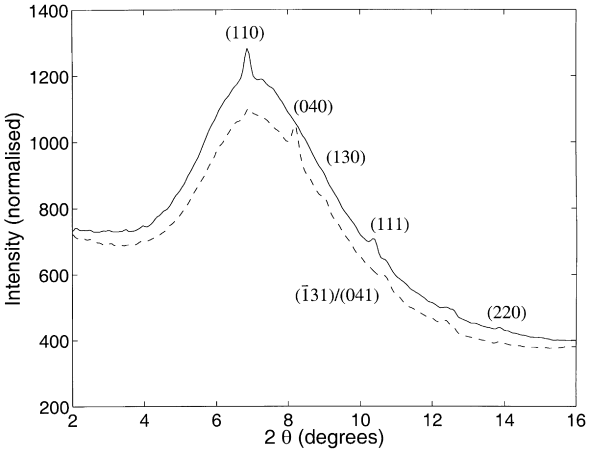

Fig. 6. Equatorial (- -) and meridional (–) WAXD intensity vs. diffraction angle 2Θ of iPP during flow at 159°C, $t = 134$ s and a low flow rate $\dot{\gamma} = 9.1\ s^{-1}$.

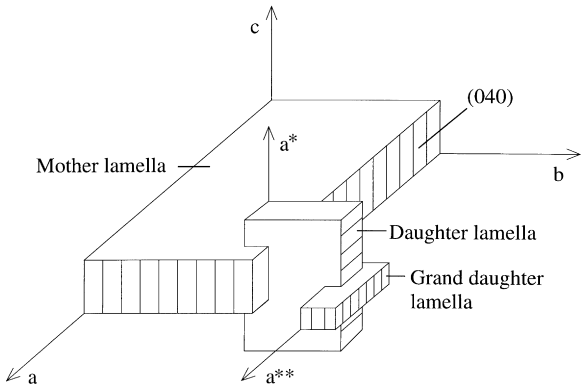

Fig. 7. Scheme of lamellar branching.

However, contrary to a low flow rate of $\dot{\gamma} = 11.8\ s^{-1}$ the resulting ordered structure at a medium flow rate of $\dot{\gamma} = 39.1$ and $67.3\ s^{-1}$ is thermally stable and does not melt with time at 161°C. Obviously, a certain flow rate is required to form a thermally stable crystalline structure. This is in agreement with the results of Katayama et al. [37] who investigated the melt spinning of polypropylene fibers by means of on-line WAXD experiments. They observed first the *c*-axis orientation and at a later time

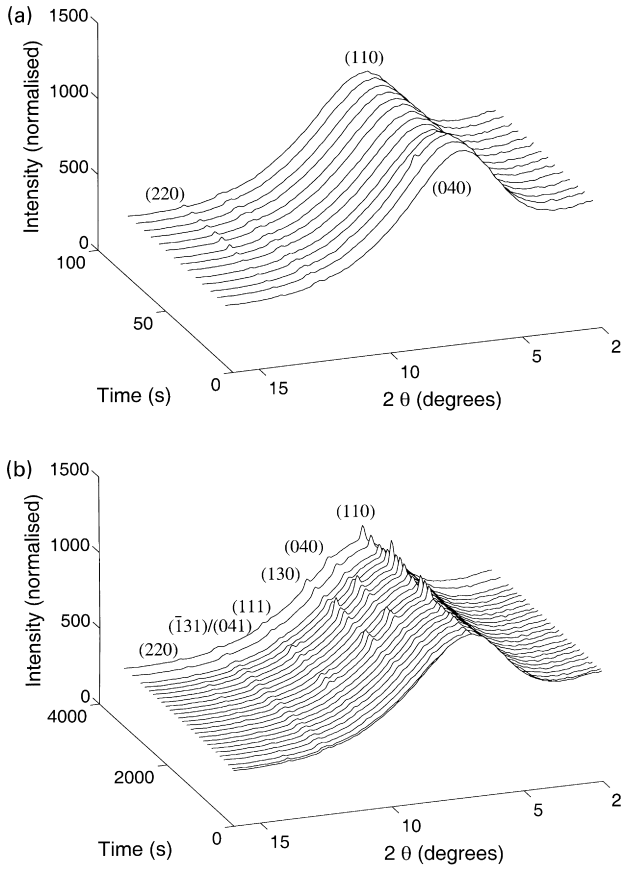

Fig. 8. Equatorial WAXD intensity of iPP vs. diffraction angle 2Θ and time (a) time range 0–80 s and (b) after flow at 161°C and a medium flow rate $\dot{\gamma} = 67.3\ s^{-1}$.

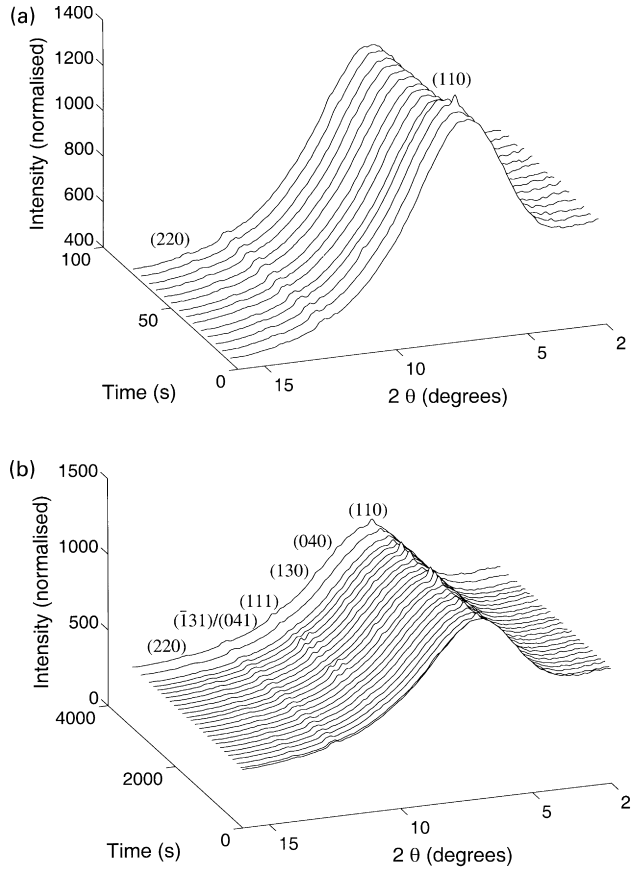

Fig. 9. Meridional WAXD intensity of iPP vs. diffraction angle 2Θ and time (a) time range 0–80 s and (b) after flow at 161°C and a medium flow rate $\dot{\gamma} = 67.3\ s^{-1}$.

further along the spinning line the a^*-axis orientation. Moreover, they reported about a lower melting temperature of the a^*-axis crystals compared to that of the c-axis crystals.

3.2.3. High flow rate

The applied high flow rates ($110.3 \leq \dot{\gamma} \leq 127.1\ s^{-1}$) limit the observation time for crystallization during the duration of flow to about 12 s. That means that crystallization can only be visualized in the case of a very high crystal growth rate. The results show no crystallization during flow; obviously the available time of 12 s was too short.

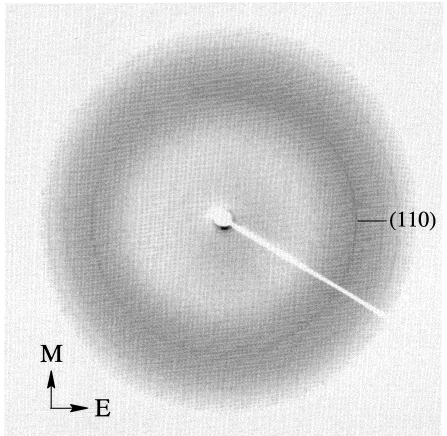

Fig. 10. 2D WAXD pattern of iPP 3035 s subsequent to flow at 161°C and a medium flow rate $\dot{\gamma} = 67.3\ s^{-1}$. The flow direction is vertical.

Significant crystallization (20–45 min) subsequent to flow first becomes visible at 163°C and $\dot{\gamma} = 110.3\ s^{-1}$. The strongest reflections are the equatorial (110), (040) and (130) reflections and the meridional (040) reflections which characterizes a preferential crystallite orientation in flow direction.

A further decrease in the flow temperature enhances crystallization, indicated by a decrease in the onset of crystallization as well as an increase in the crystalline content. For example, the onset of crystallization decreases from 60 to 27 s (subsequent to flow) with a decrease in temperature from 161 to 159°C.

Fig. 12 represents a 2D pattern which is obtained at 3082 s subsequent to flow at 161°C and applying a high flow rate of $\dot{\gamma} = 124.0\ s^{-1}$. Such a time coincides with the longest observation time and consequently, documents the largest attainable degree of crystallinity. Obviously there is a significant arcing of the three equatorial reflections (110), (040) and (130). The corresponding intensity distribution along the equator as well as meridian is seen in Fig. 13 which indicates the existence of a monoclinic α-modification and a strong anisotropy. The equatorial intensities are much stronger than those along the meridian, explained by a preferred crystallite orientation in flow direction.

The crystallization behavior at 159°C and $\dot{\gamma} = 127.1\ s^{-1}$ is similar to that at 161°C and $\dot{\gamma} = 124.0\ s^{-1}$. However, the crystal growth rate at 159°C is more pronounced due to the larger undercooling $T_m^0 - T_c$. Figs. 14 and 15 represent the time-dependent formation of the crystalline WAXD reflections along the equator as well as the meridian. It is apparent the onset of crystallization of about 27 s and a steady growth in the peak intensities thereafter. The high flow rate has strongly forced the molecules to align parallel to the main flow direction. As a consequence, the equatorial reflections are more intense than the corresponding meridional ones which is also seen in the 2D plot in Fig. 16.

A low flow rate induces a molecular ordering during flow at temperatures as high as 170°C, which is far above the crystallization range under quiescent conditions. The crystalline intensities increase with time, reach a maximum in the time range from about 95 to 140 s and vanish afterwards. The observed arcing of the intense meridional (110) and equatorial (040) reflections may be a consequence of a lamellar branching of crystallites in the daughter lamella with their a^*-axis in flow direction.

At medium flow rates at 161°C an onset of crystallization with the formation of (110) and (040) reflections is observed at about 17 s, i.e. during flow. The (110) reflection with a simultaneous arcing along the equator as well as the meridian are characteristic for the existence of a lamellar branching as previously seen at low flow rates. Subsequent

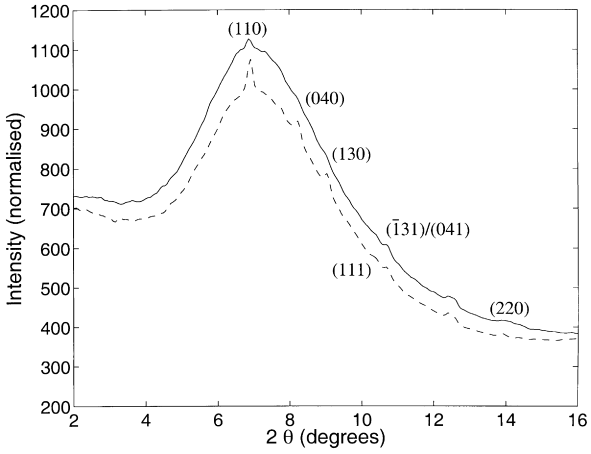

Fig. 11. Equatorial (- -) and meridional (–) WAXD intensity vs. diffraction angle 2Θ of iPP 3035 s subsequent to flow at 161°C and a medium flow rate $\dot{\gamma} = 67.3\ s^{-1}$.

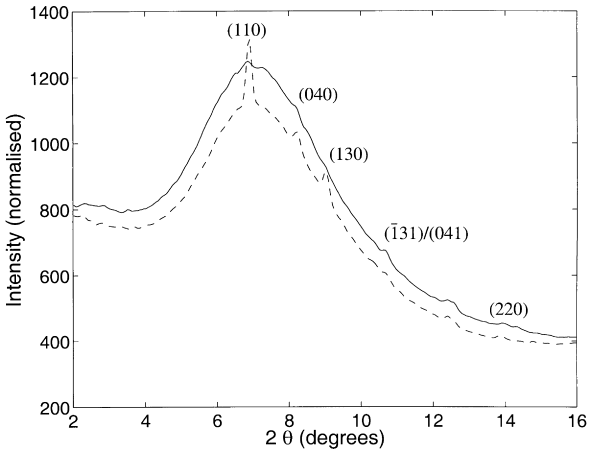

Fig. 13. Equatorial (- -) and meridional (–) WAXD intensity vs. diffraction angle 2Θ of iPP 3082 s subsequent to flow at 161°C and a high flow rate $\dot{\gamma} = 124.0\ s^{-1}$.

to flow, a steady crystal growth with time has been monitored. The crystal structure is thermally stable in the entire time range subsequent to flow and reaches a maximum intensity at the end of the 60 min observation. The final crystalline structural represents intense equatorial (110), (040) and (130) reflections which indicates an alignment of crystallites with their *c*-axis in flow direction.

High flow rates have limited the observation time during flow down to about 12 s which is too short to detect crystallization. Significant crystal growth subsequent to flow occurs at 163°C and below. A decrease in temperature causes a decrease in the onset of crystallization together with an increase in the degree of crystallinity. The onset of crystallization changes from 20 to 45 min (163°C) to 60 s (161°C) and 27 s (159°C) subsequent to flow due to the larger undercooling $T_m^0 - T_c$. The high flow rate has strongly forced the molecules to align parallel to the main flow direction, resulting in an intense arcing of the (110), (040) and (130) reflections along the equator.

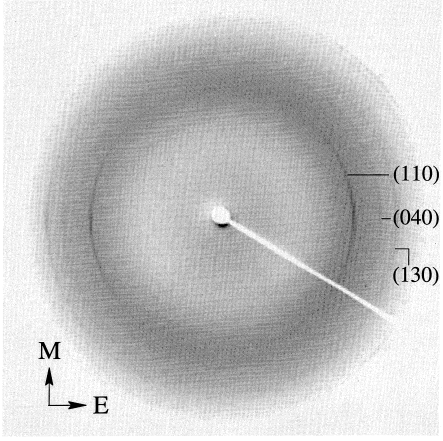

Fig. 12. 2D WAXD pattern of iPP 3082 s subsequent to flow at 161°C and a high flow rate $\dot{\gamma} = 124.0\ s^{-1}$. The flow direction is vertical.

4. Conclusions

Time-resolved 2D WAXD measurements using iPP have been performed in order to investigate crystal growth and crystallite orientation during and subsequent to melt flow as

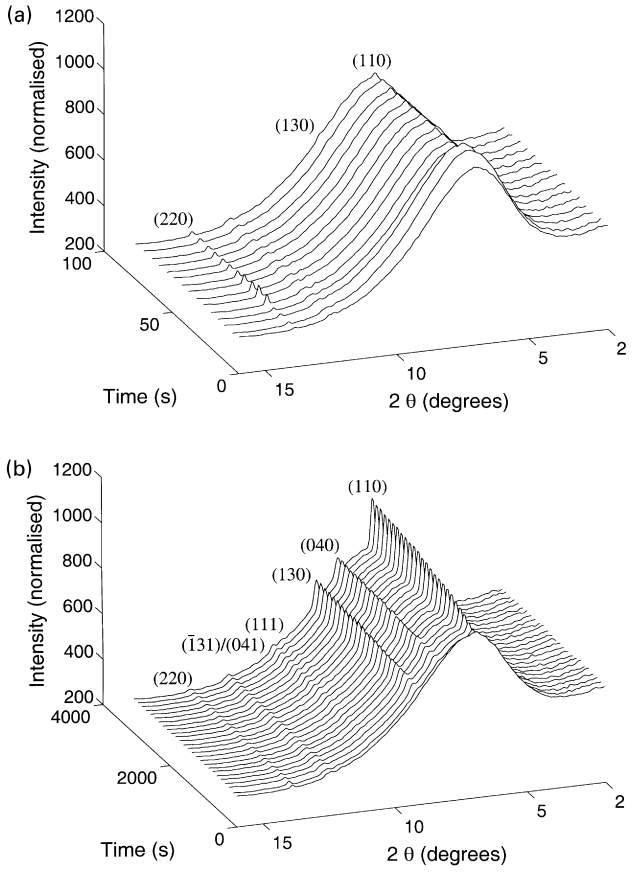

Fig. 14. Equatorial WAXD intensity of iPP vs. diffraction angle 2Θ and time (a) time range 0–80 s and (b) subsequent to flow at 159°C and a high flow rate $\dot{\gamma} = 127.1\ s^{-1}$.

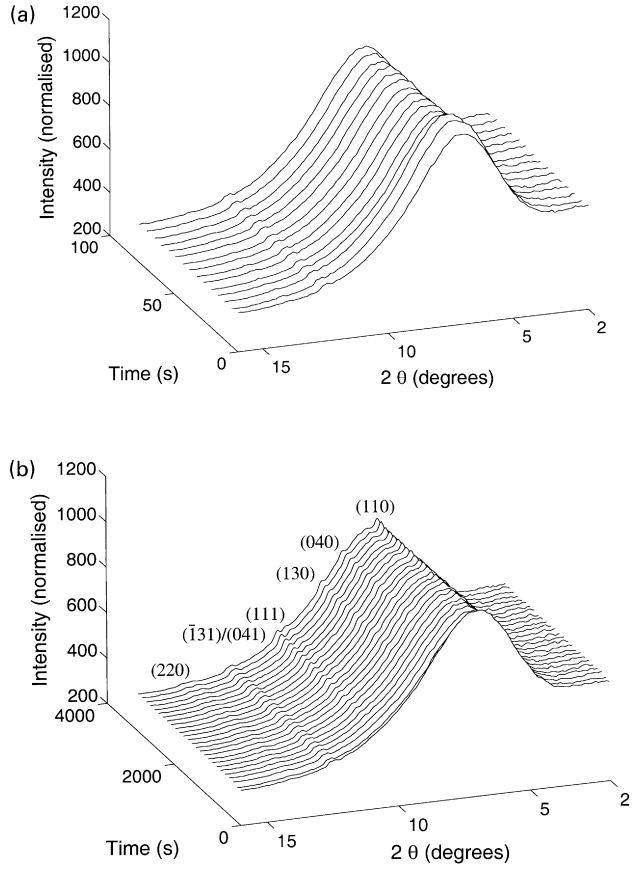

Fig. 15. Meridional WAXD intensity of iPP vs. diffraction angle 2Θ and time (a) time range 0–80 s and (b) subsequent to flow at 159°C and a high flow rate $\dot{\gamma} = 127.1\ s^{-1}$.

a consequence of conformational changes herewith. Prior to flow, an annealing procedure was carried out at 230°C and 90 min to erase memory effects associated with clusters, crystal aggregates and molecular conformations. Thereafter, the iPP melt was cooled down to the anticipated crystallization (flow) temperature and finally, forced through a contraction zone in the flow cell. Each single experiment was performed at a certain flow temperature, varied in 2°C-steps in the range from 159 to 172°C and at a flow rate, classified as low ($9.1 \leq \dot{\gamma} \leq 16.0\ s^{-1}$), medium ($39.1 \leq \dot{\gamma} \leq 67.3\ s^{-1}$) and high ($110.3 \leq \dot{\gamma} \leq 127.1\ s^{-1}$). The WAXD patterns were recorded during the duration of flow (12–165 s) with a acquisition time as short as about 5 s and subsequent to flow up to at least 60 min.

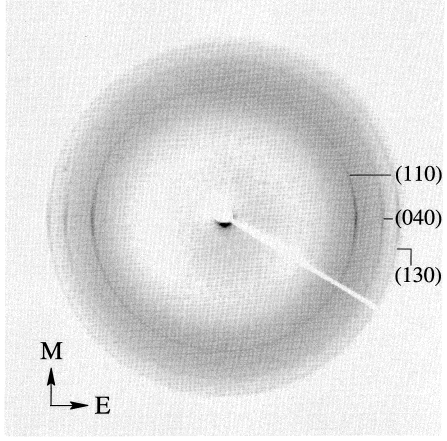

Fig. 16. 2D WAXD pattern of iPP 3082 s subsequent to flow at 159°C and a high flow rate $\dot{\gamma} = 127.1\ s^{-1}$. The flow direction is vertical.

Acknowledgements

Financial support of the DECRYPO (Brite-EuRam III) program and Philips Research is gratefully acknowledged. The authors would like to thank Prof. A. Keller, Bristol University, UK for the fruitful discussions on the subject and Dr J.W.H. Kolnaar from DSM, Geleen for putting the flow cell available. We appreciate the use of the ID11-BL2 beamline at the European Synchrotron Radiation Facility (ESRF) in Grenoble, France and the technical assistance of Dr. P. Rejmankova-Pernot (ESRF) and H. Wilderbeek (TU Eindhoven). The iPP material was provided by Borealis AG, Linz, Austria and kindly prepared in rod-shaped preforms by Dr. H. Wippel from the University of Linz.

References

[1] Liedauer S, Eder G, Janeschitz-Kriegl H, Jerschow P, Geymayer W, Ingolic E. Int Polym Process 1993;8:236.
[2] Eder G, Janeschitz-Kriegl H, Liedauer S. Prog Polym Sci 1990;15:629.
[3] Meijer HEH, editor. Material sciences and technology: part II, 18. Weinheim: Verlag Chemie, 1997. p. 5.
[4] Karger-Kosics J, editor. Polypropylene, structure, blends and composites: part II, 1. London: Chapman & Hall, 1995.
[5] Mackley MR, Keller A. Polymer 1973;14:16.
[6] Mackley MR, Keller A. Phil Trans Roy Soc London. Ser A 1975;278:29.
[7] Mackey ME, Dajan AM, Wippel H, Janeschitz-Kriegl H, Lipp M. J Rheol 1995;39:1.
[8] Vleeshouwers S, Meijer HEH. Rheol Acta 1996;35:391.
[9] Isayev AI, Chan TW, Shimojo K, Gmerek M. J Appl Polym Sci 1995;55:807.
[10] Mackley MR, Frank FC, Keller A. J Mater Sci 1975;10:1501.
[11] Kolnaar JWH, Keller A, Seifert S, Zschunke C, Zachmann HG. Polym Commun 1955;36:3969.
[12] Natta G, Corradini P. Nuovo Cim 1960;Suppl. 15:40.
[13] Turner-Jones A, Aizlewood JM, Beckett DR. Makromol Chem 1964;75:134.
[14] Zipper P, Janosi A, Wrentschur E, Abuja PM, Knabl C. Prog Colloid Polym Sci 1993;93:377.
[15] Padden FJ, Keith HD. J Appl Phys 1959;30:1479.
[16] Lovinger AJ, Jaime OC, Gryte CC. J Polym Sci: Polym Phys Ed 1977;15:541.
[17] Vleeshowers S. Polymer 1997;38:3213.
[18] Pae KD, Sauer JA, Morrow DR. Nature 1966;211:514.
[19] Morrow DR, Newmann BA. J Appl Phys 1968;39:4944.
[20] Lotz B, Graff S, Wittmann JC. J Polym Sci Part B: Polym Phys 1986;24:2017.
[21] Clark ES, Spruiell JE. Polym Engng Sci 1976;16:176.

[22] Brückner S, Meille SV, Petraccone V, Pirozzi B. Prog Polym Sci 1991;16:361.
[23] Padden FJ, Keith HD. J Appl Phys 1966;37:4013.
[24] Lotz B, Wittmann JC, Lovinger AJ. Polymer 1996;37:4979.
[25] Khoury F. J Res Nat Bur Stand 1966;A70:29.
[26] Lotz B, Wittmannn JC. J Polym Sci: Polym Phys Ed 1986;24:1541.
[27] Yamada K, Matsumoto S, Tagashira K, Hikosaka M. Polymer 1998;39:5327.
[28] Terril NJ, Fairclough PA, Towns-Andrews E, Komanschek BU, Young RJ, Ryan AJ. Polymer 1998;39:2381.
[29] Olmsted PD, Poon WCK, McLeish TCB, Terrill NJ, Ryan AJ. Phys Rev Lett 1998;81:373.
[30] Product Information, PCD GmbH, Linz, Austria.
[31] Process Information, University of Linz, Austria.
[32] Alfonso GC, Ziabicki A. Colloid Polym Sci 1995;273:317.
[33] Hammersly AP, Svensson SO, Thomson A. Nucl Instr Methods Phys Res 1994;A346:321.
[34] Göschel U, Swartjes F, Peters GWM, Meijer HEH. Unpublished.
[35] Bu HS, Cheng ZD, Wunderlich B. Makromol Chem Rapid Commun 1988;9:75.
[36] Nakafuku C. Polymer 1981;22:1673.
[37] Katayama K, Amano T, Nakamura K. Kolloid Z-Z Polym 1968;226:125.